The following publication Kai Wang and Zhongqing Su "Analytical modeling of contact acoustic nonlinearity of guided waves and its application to evaluating severity of fatigue damage", Proc. SPIE 9805, Health Monitoring of Structural and Biological Systems 2016, 98050L (1 April 2016) is available at https://doi.org/10.1117/12.2218705.

Analytical modeling of contact acoustic nonlinearity of guided waves and its application to evaluating severity of fatigue damage

Kai Wang and Zhongqing Su*
Department of Mechanical Engineering, The Hong Kong Polytechnic University, Kowloon Hong Kong SAR

ABSTRACT

Targeting quantitative estimate of fatigue damage, a dedicated analytical model was developed based on the modal decomposition method and the variational principle. The model well interprets the contact acoustic nonlinearity induced by a "breathing" crack in a two-dimensional scenario, and the nonlinear characteristics of guided ultrasonic waves (GUWs) (*e.g.*, reflection, transmission, mode conversion and high-order generation) when GUWs traversing the crack. Based on the model, a second-order reflection index was defined. Using the index, a fatigue damage evaluation framework was established, showing demonstrated capacity of estimating the severity of fatigue damage in a quantitative manner. The approach, in principle, does not entail a benchmarking process against baseline signals pre-acquired from pristine counterparts. The results obtained using the analytical modeling were compared with those from finite element simulation, showing good coincidence. Limitations of the model were also discussed.

Keywords: "breathing" crack, guided ultrasonic waves, analytical model, contact acoustic nonlinearity

1. INTRODUCTION

Engineering structures, particularly transportation vehicles, undergo repetitive loading and unloading processes during their service life, and under this they are susceptible to fatigue damage which is initiated by material defects or sharp change in structural geometry. Without timely awareness and early prevention, the fatigue damage can grow rapidly to a critical point to threaten the overall integrity of the structures, accordingly causing huge economic cost and even loss of life. Catastrophic disasters witnessed over the past few decades have entailed intensive research and development of methods to detect the presence of fatigue damage at an early stage. As reported in rich literature[1-5], various methods and strategies, using guided ultrasonic waves (GUWs), have been deployed for evaluation of fatigue damage and extended to structural health monitoring. The majority of these methods and strategies fall into a category of linear techniques, by which the damage is characterized by canvassing the signal features at the frequency of incident energy, such as time-of-flight, reflection/ transmission and mode conversion. These methods can provide effective damage identification when fatigue damage causes conspicuous alternations in linear features. However, practical applications have confirmed that the linear techniques are capable of only discerning damage with characteristic scale comparable with the wavelength of the probing waves[6-10], and thus they may fail to infer fatigue damage (*e.g.*, fatigue crack) which barely affects GUWs propagation at the frequency of incident energy. In addition, complex structural boundaries can cause multi-reflections which might disturb the detectability of these linear approaches. Due to high sensitivity to damage of small scale, a great deal of effort has been directed to investigating and developing nonlinear techniques, with a hope to detect small-scale damage by exploiting the shift of energy from the incident frequency to other frequency bands.

A large majority of existing nonlinear methods interpret the nonlinearity introduced into GUWs by damage, via making use of a classical nonlinearity model[11-15], which attributes the distortion of probing waves and generation of high-order harmonics – a typical nonlinear property of GUWs – to the nonlinear stress-strain relation of the material. In an intact status, this type of nonlinearity is related to the anharmonicity of interatomic potential, which under most circumstances is barely perceivable. Provided the synchronism requirements[11] are met, the nonlinear features of GUWs can be observed to accumulate along a wave propagating path. On the contrary, material fatigue can induce plasticity, which strengthens

* Zhongqing.Su@polyu.edu.hk; phone +852-2766-7818; fax +852-2365-4703

the nonlinearity. However, the limitations imposed by the synchronism requirements are also evident: the fatigue plasticity-driven model can only infer the presence of material fatigue, but fails to localize the site of potential fatigue damage, because the model is unable to depict faithfully the plasticity in the vicinity of a fatigue damage. Provided a fatigue crack is present in the medium, it is more appropriate to use the contact acoustic nonlinearity (CAN) model[16] (the so-called "breathing" crack) for interpreting the modulation mechanism of the crack on probing GUWs propagation and generation of high-order harmonics. In most cases, the CAN-induced nonlinearity dominates nonlinear signal features, while the material plasticity-driven nonlinearity is insignificant. Solodov *et al.*[16] scrutinized the interaction between a "breathing" crack and an incident wave using a model addressing CAN introduced by the crack. This model assumed a step-change of stiffness in material at the site of crack, whereby this model offers a rational explanation for the generation of high-order harmonics in a quantitative manner when probing waves traversing the crack. However, the model is developed based on a premise that the strain field at the crack is calculated by the incident wave only, which has a constant magnitude yet without considering the influence of the waves scattered by the crack. In practice, in order to strengthen crack-induced nonlinearity, another method[17-20] based on CAN was developed which modulated the probing wave with a low frequency yet high magnitude vibration. The vibration excitation forces the crack to open and close, and in the meanwhile a GUW signal is applied to be modulated by the vibration, leading to presence of sidebands in frequency spectrum. By doing this, nonlinear features of GUWs induced by the crack can be enhanced. Experimental verification has demonstrated that this method is applicable to establishment of a correlation between nonlinear features and crack parameters. Essentially, these methods abovementioned make use of the modulation of CAN on traversing waves for evaluation of fatigue cracks. However, lacking of in-depth understanding of the modulation mechanism of CAN on GUWs makes these techniques ineffective towards quantitative estimate of fatigue cracks. The paramount challenge for obtaining analytical explanation of modulation mechanism of the "breathing" crack on GUWs is attributed to the time-varying nature of the boundary condition of the "breathing" crack when GUWs traversing.

Motivated by this, in this study we developed a dedicated analytical model which is able to interpret the modulation mechanism of CAN of a "breathing" crack on GUWs and generation of high-order harmonics. The model interprets nonlinearity induced by the "breathing" crack in a two-dimension (2D) scenario. Based on the modal decomposition method and the variational principle, this model establishes a framework in which a second-order nonlinear index was defined, to estimate the severity of fatigue damage quantitatively. Validation of the model was implemented by comparing the results with those from finite element simulation. The paper is organized as follows: modulation mechanism of CAN on GUWs propagation and dynamic behaviors of the "breathing" crack" in time domain are investigated and detailed in Section 2. In this section, a correlation between CAN-based nonlinear index and crack severity is also developed. Validation of the index using finite element simulation is reported in Section 3. Potential limitations of the proposed method are discussed in Section 4 with concluding remarks.

2. MODULATION MECHANISM OF CAN ON GUWS PROPAGATION AND GENERATION OF HIGH-ORDER HARMONICS

A "breathing" crack can be deemed as a second source in the medium to excite an additional wave field when probing waves are traversing through it, and this source accordingly introduces deviation in the wave field from that in an intact case. Subsequently, the corresponding "crack-induced second-source-stress loading" (hereafter CISS) serves as an excitation source for scattered waves. In the model as shown in Figure 1, when a surface "breathing" crack is present in a 2D infinite medium, the plate can be simulated using two semi-infinite plates bonded together at the site of the crack. The CISS on the edge of each semi-infinite plate (Edge I, and Edge II as shown in the figure) accounts for the deviation.

Considering the time-varying nature of the boundary conditions when the crack "breathes", the duration for the crack to complete an open-close cycle (in the time domain) and the cross-thickness distribution (in the spatial domain) of CISS are prerequisites for determination of reflection/transmission of GUWs at the fundamental frequency and high-order frequencies. To acquire the duration, the crack "breathing" behaviors (*i.e.* closing and opening) were scrutinized by

exploiting a modal decomposition method. The propagating wave mode generated by the CISS was analyzed by using a variational principle-based method.

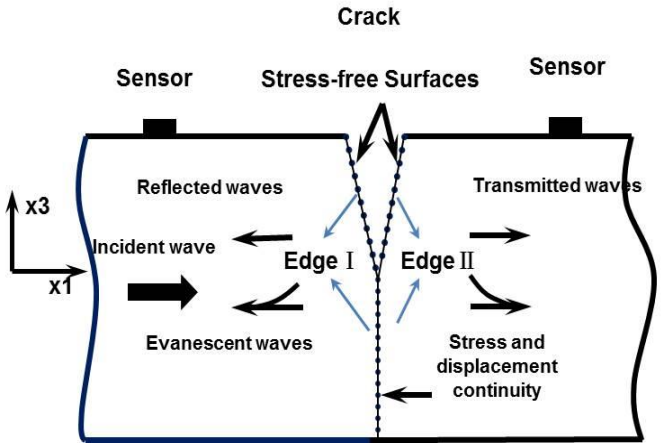

Figure 1. Schematic of a 2D infinite plate bearing a "breathing" crack when crack is open

2.1 Contacting behavior of "breathing" crack

When the crack closes, compressive and shear stress of propagating GUWs are transmitted; and when the crack opens during dilation, waves are partially decoupled. These will jointly lead to different stress-strain relations at the crack interface, reflecting the "breathing" behavior of the fatigue crack under the modulation of propagating GUWs. In this method, the stress field at the crack is jointly determined by the incident and scattered waves. Furthermore, it is the superposed wave field that governs the time period during which the CISS presents. When the crack is closed, waves propagate in the same fashion as in an intact plate and the superposed stress field is identical to that of the incident wave due to the disappearance of the crack-induced deviation. Under this condition the displacement at the crack can be described by the incident displacement field. When the tensile phase of the incident wave arrives, denoted by t_{open}, the crack is open and it induces wave scattering, and afterward the crack interfaces behave in an identical manner as the case that GUWs traverse a fully opened notch with the same depth.

During the process of crack opening, crack behavior and the CISS can be obtained by using a modal decomposition method[21, 22]. This method is based on the premise that the propagating and evanescent wave modes compose a complete basis, and superposition of these modes yields the stress or displacement of arbitrary cross-thickness distribution[23]. Solving the dispersive Equation (1) by using a Newton-Raphson method gives a finite number of real roots (propagating modes) and pure imaginary roots, along with an infinite number of complex roots (evanescent modes), as shown in Figure 2

$$\frac{\tan(qh)}{\tan(ph)} = \frac{4k^2 qp\mu}{\left(\lambda k^2 + \lambda p^2 + 2\mu p^2\right)\left(k^2 - q^2\right)}. \tag{1}$$

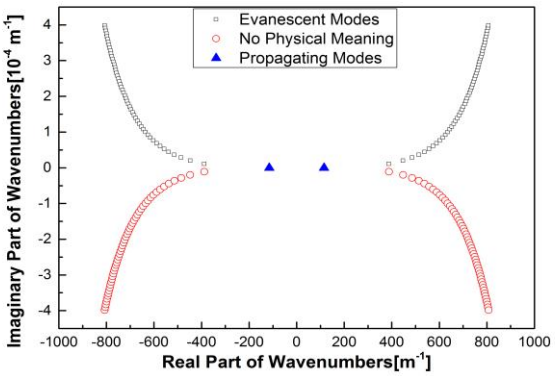

Figure 2. Roots for dispersive equation in a complex wavenumber domain

As said in the above, the stress field and displacement field can be expanded as the superposition of propagating modes and evanescent modes induced by incident waves and crack-scattered waves,

$$u = \sum\nolimits_n b_n u^n \quad and \quad \sigma = \sum\nolimits_n b_n \sigma^n, \tag{2}$$

where $u^n = u^n\left(x_3\right)e^{i(\omega t - kx_1)}$ and $\sigma^n = \sigma^n\left(x_3\right)e^{i(\omega t - kx_1)}$, which are the displacement vector and stress tensor for the n^{th} wave Lamb mode, respectively. t is the time, and k the wavenumber.

Thus, when the crack is open, as shown in Figure 1, the boundary conditions[21] of the crack can be described as

$$\begin{matrix}\sigma_{11}\\ \sigma_{13}\end{matrix} = \begin{cases}\sum_N b_N \sigma_{11}^N\\ \sum_N b_N \sigma_{13}^N\end{cases} = \begin{cases}0\\ 0,\end{cases} \text{ stress free at the right surface of crack} \tag{3}$$

$$\begin{matrix}\sigma_{11}\\ \sigma_{13}\end{matrix} = \begin{cases}b_{Inc}\sigma_{11}^{Inc} + \sum_N b_{-N}\sigma_{11}^{-N}\\ b_{Inc}\sigma_{13}^{Inc} + \sum_N b_{-N}\sigma_{13}^{-N}\end{cases} = \begin{cases}0\\ 0,\end{cases} \text{ stress free at the left surface of crack} \tag{4}$$

$$\sum\nolimits_N b_N u^N = b_{Inc}u^{Inc} + \sum\nolimits_N b_{-N}u^{-N}, \text{ displacement continuity out of crack} \tag{5}$$

$$\begin{matrix}\sum_N b_N \sigma_{11}^N\\ \sum_N b_N \sigma_{33}^N\\ \sum_N b_N \sigma_{13}^N\end{matrix} = \begin{cases}b_{Inc}\sigma_{11}^{Inc} + \sum_N b_{-N}\sigma_{11}^{-N}\\ b_{Inc}\sigma_{33}^{Inc} + \sum_N b_{-N}\sigma_{33}^{-N}\\ b_{Inc}\sigma_{13}^{Inc} + \sum_N b_{-N}\sigma_{13}^{-N}.\end{cases} \text{ stress continuity out of crack} \tag{6}$$

In the above, N is the index of propagating and evanescent modes, and a negative N indicates the modes propagating opposite to the incident wave. Coefficient b_N is the unknown complex magnitude to be correlated with the magnitude of incident wave which is denoted by b_{Inc} . σ^{Inc} and u^{Inc} are the stress and displacement fields induced by incident waves, respectively.

Upon solving Equations (3)-(6) using a singular value decomposition method, the magnitude of each mode can be obtained and therefore the displacement and stress fields at the crack can be depicted as follows:

$$\begin{aligned} u_1^- \left(x_3, t \right) &= b_{Inc} u^{Inc} + \sum\nolimits_N b_{-N} u^{-N} \\ \sigma_{11}^{Crack-} &= b_{Inc} \sigma_{11}^{Inc} + \sum\nolimits_N b_{-N} \sigma_{11}^{-N} \quad \text{at the left edge of the crack} \\ \sigma_{13}^{Crack-} &= b_{Inc} \sigma_{13}^{Inc} + \sum\nolimits_N b_{-N} \sigma_{13}^{-N}, \end{aligned} \tag{7}$$

$$\begin{aligned} u_1^+ \left(x_3, t \right) &= \sum\nolimits_N b_N u^N \\ \sigma_{11}^{Crack+} &= \sum\nolimits_N b_N \sigma_{11}^N \quad \text{at the right edge of the crack} \\ \sigma_{13}^{Crack+} &= \sum\nolimits_N b_N \sigma_{13}^N . \end{aligned} \tag{8}$$

Accordingly, the CISS when the crack opens can be yielded as:

$$\begin{aligned} \sigma_{11}^{CISS\pm} &= \sigma_{11}^{Crack\pm} - \sigma_{11}^{Inc} \\ \sigma_{13}^{CISS\pm} &= \sigma_{13}^{Crack\pm} - \sigma_{13}^{Inc} . \end{aligned} \tag{9}$$

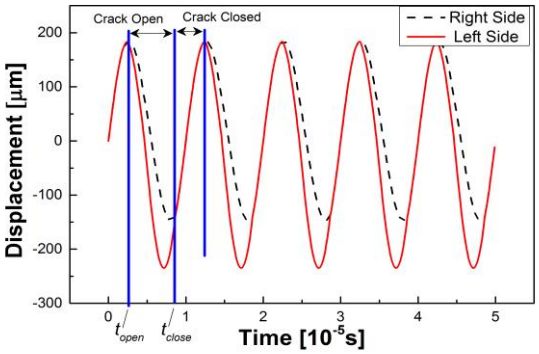

(a)

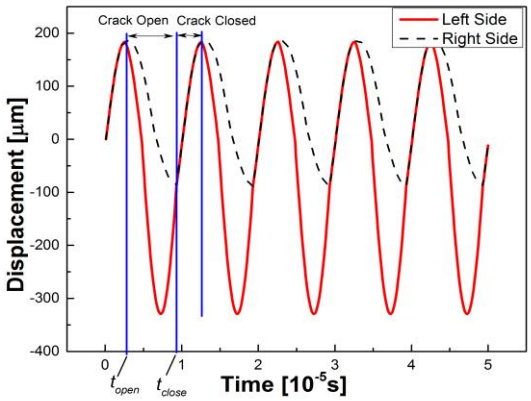

(b)

Figure 3. Displacement history of concerned points when ratio of the crack depth to plate thickness is (a) 50%; and (b) 75%

Based on the respective displacement fields at the left and right stress-free surfaces of the crack, setting the gap between two stress-free surfaces as zero yields the moment when the crack closes and therefore wave scattering from the crack edge vanishes, as depicted by Equation (10). Upon closing, the procedure of the crack opens/closes repeats periodically. For illustration, Figure 3 shows the displacement history diagrams of two representative points which are on the left and right stress-free surfaces of the crack sharing the same original position in plate thickness.

$$u_1^+\left(x_3, t_{close}\right) - u_1^-\left(x_3, t_{close}\right) = 0, \tag{10}$$

where $u_{x_1}^+\left(x_3\right)$ and $u_{x_1}^-\left(x_3\right)$ denote the displacements of the two points along x_1 axis on the right (transmitted) and left (reflected) stress-free surface of crack, respectively. Solving Equation (10) gives the time t_{close} when crack closes. Therefore, the CISS, defined as the deviation of crack-induced stress field from that of incident wave, is present during crack opening and absent otherwise. This phenomenon can be treated as the scenario in which the crack-induced stress in an open crack case is modulated by a periodic window function, as

$$f\left(t\right) = \begin{cases} 1, & t_{open} < t < t_{close} \\ 0, & t_{close} < t < t_{open} + T. \end{cases} \tag{11}$$

Therefore, the CISS can be obtained as:

$$\begin{aligned} \sigma_{11}^{CISS\pm} &= \left(\sigma_{11}^{Crack\pm}\left(x_3\right) - \sigma_{11}^{Inc}\left(x_3\right)\right)\mathrm{e}^{iwt} \times f\left(t\right) \\ \sigma_{13}^{CISS\pm} &= \left(\sigma_{13}^{Crack\pm}\left(x_3\right) - \sigma_{13}^{Inc}\left(x_3\right)\right)\mathrm{e}^{iwt} \times f\left(t\right). \end{aligned} \tag{12}$$

The corresponding frequency spectra of the CISS can be obtained using the convolution between the incident wave period function e^{iwt} and window function $f\left(t\right)$, leading to the magnitude of each frequency component. To summarize, the above process can be illuminated in Figure 4.

By extracting the magnitude of the second harmonic from the spectra, denoted by A_{2f_0}, the CISS at the double frequency can be obtained, as

$$\begin{aligned} \sigma_{11}^{CISS-2f_0} &= A_{2f_0}\left(\sigma_{11}^{Crack}\left(x_3\right) - \sigma_{11}^{Inc}\left(x_3\right)\right)e^{i2wt} \\ \sigma_{13}^{CISS-2f_0} &= A_{2f_0}\left(\sigma_{13}^{Crack}\left(x_3\right) - \sigma_{13}^{Inc}\left(x_3\right)\right)e^{i2wt}. \end{aligned} \tag{13}$$

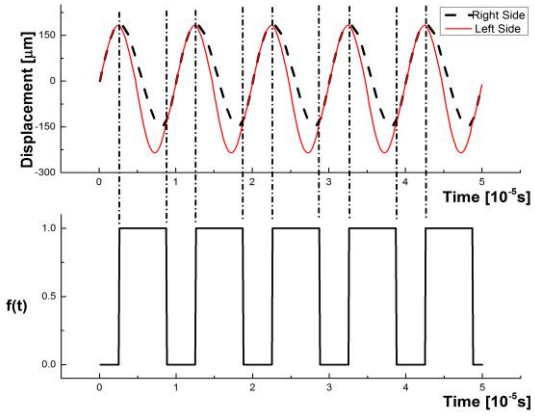

(a)

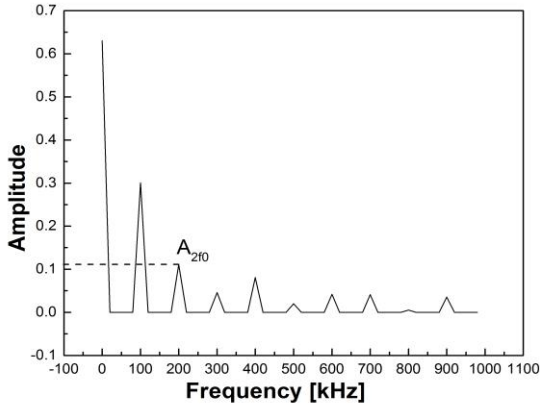

(b)

Figure 4. (a) Modulation function based on Eq. (11); and (b) Spectrum of calculated CISS

To this point, the CISS has been obtained and the investigation of original time-varying interaction between the probing waves and the "breathing" crack is proceeded to the study of a time-invariant boundary excitation for two semi-infinite plates.

2.2 Wave mode generation method based on Variational Principle

In order to achieve an insight into the consequently generated propagating second harmonic components in the reflection/transmission wave fields, a method based on the variational principle was employed. In this method, the obtained distribution of CISS is applied on the left edge of the semi-infinite plate left to the crack, as shown in the Figure 5. The accordingly induced wave modes can be described using variational principle[24,25]. As mentioned above, the resulting stress and displacement fields of the excited wave modes are namely the superposition of those of available wave modes, respectively, including propagating and evanescent modes. The same as stated in Equation (2), b_n is the magnitude of the n^{th} excited mode. On the edge, when the magnitude b_n of each mode is properly calculated, the stress at $x_1 = 0$ becomes

$$\begin{aligned} T_1 &= \sum b_n \sigma_{11}^n = \sigma_{11}^{CISS-2f_0}\left(x_3, t\right) \\ T_3 &= \sum b_n \sigma_{13}^n = \sigma_{13}^{CISS-2f_0}\left(x_3, t\right). \end{aligned} \tag{14}$$

For the discussed plate, according to the variational principle, it has

$$\int_V \left(\sigma_{ik,k} - \rho \ddot{u}_i\right) \delta u_i dv + \int_S \left(T_i - \hat{x}_i \sigma_{ki}\right) \delta u_i ds = 0. \tag{15}$$

In the above, V denotes volume and S surface. Given the stress and displacement fields can be regarded as the superposition of the wave modes in an infinite plate, the volume integral, the first term on the left side of the equation, vanishes when wave mode satisfies the differential equations of equilibrium.

Based on Equation (2), it has

$$\delta u_i = \sum \delta\left(b_m\right) \bullet u_i^m. \tag{16}$$

Substituting Equations (14) and (16) into the surface integral, we have

$$\int_S \left[T_i - \hat{x}_k \sum_n b_n \bullet \sigma_{ki}^n e^{ikx_1} \right] e^{-i2\omega t} \bullet \left[\delta(b_m) \bullet u_i^m e^{ikx_1} \right] e^{-i2\omega t} ds = 0. \tag{17}$$

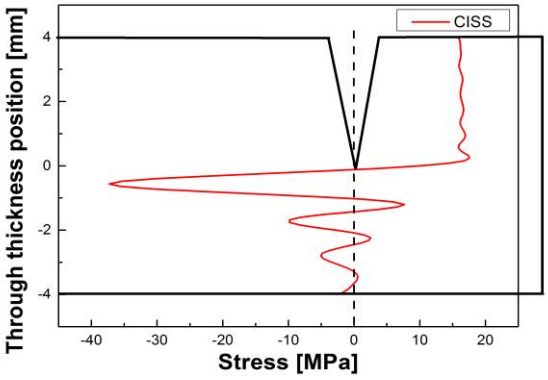

Figure 5. Cross-thickness distribution of CISS

Averaging Equation (17) over a complete period of the high-order harmonic mode and solving the equation at the edge $x_1 = 0$ yields

$$\int_{-h}^{h} \left[\bar{T}_i - \hat{x}_k \bullet b_n \bullet \bar{\sigma}_{ki}^n \right] \delta(b_m) \bullet u_i^m dx_3 = 0. \tag{18}$$

Equation (18) is tenable when

$$\frac{1}{h} \int_{-h}^{h} \left(u_1^m \bar{T}_1 + u_3^m \bar{T}_3 \right) dx_3 = \frac{1}{h} \int_{-h}^{h} \left(u_1^m \bar{\sigma}_{11}^n + u_3^m \bar{\sigma}_{13}^n \right) b_n dx_3. \tag{19}$$

Now, we define

$$M_{mn} = \frac{1}{h} \int_{-h}^{h} \left(u_1^m \bar{\sigma}_{11}^n + u_3^m \bar{\sigma}_{13}^n \right) dx_3. \tag{20}$$

With the inverse of M_{mn}, denoted by $\left[R_{pm} \right]$, we have $\left[R_{pm} \right] \bullet \left[M_{mn} \right] = \delta_{pn}$. Multiplying $\left[R_{pm} \right]$ at both sides of Equation (19) gives

$$b_p = \left[R_{pm} \right] \bullet \frac{1}{h} \int_{-h}^{h} \left(u_1^m \bar{T}_1 + u_3^m \bar{T}_3 \right) dx_3. \tag{21}$$

As a matter of fact, in terms of physical interpretation, the matrix M_{mn} represents the average rate at which the stress of wave mode m does work when acting through the displacements of a mode n. The real part of $\left[M \right]$ represents reactive work, while the imaginary part stands for the real work. Substituting the expression of CISS into Equation (21) yields the magnitude of each wave mode induced by the CISS. Figure 6 compares the CISS with the superposition of correspondingly generated wave modes calculated using the variational principle-based method.

Though both propagating and evanescent modes are excited, evanescent modes transfer no energy and decay exponentially along the propagating path, and thus only the propagating mode can be detected. The first mode of the calculated results represents the generated propagating mode at second-order frequency:

$$\begin{aligned} U_1^{2f_0} &= b_1 u_1^{2f_0}\left(x_3\right) \\ U_3^{2f_0} &= b_1 u_3^{2f_0}\left(x_3\right), \end{aligned} \tag{22}$$

where $u_1^{2f_0}\left(x_3\right)$ and $u_3^{2f_0}\left(x_3\right)$ are the mode shape functions for the in-plane and out-of-plane displacements, respectively. The results show that the generated second order wave modes in the reflection and transmission packets are identical, because the CISS at double frequency are equivalent for both edges of the crack. This implies that, in principle, characterization of the crack using the second harmonic mode acquired by either "pulse-echo" or "pitch-catch" sensing configuration is equally feasible, with comparable precision.

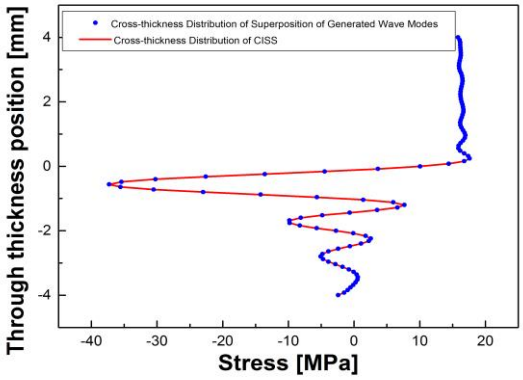

Figure 6. Comparison between excitation (using CISS) and response (superposed wave modes)

With the signal captured using "pulse-echo" sensing configuration, a dimensionless nonlinearity-based damage index was proposed, to be linked to the severity of fatigue crack:

$$NI = \frac{U_1^{2f_0}}{U_1^{f_0}} = \frac{b_1 u_1^{2f_0}\left(x_3\right)}{b_{Inc} u_1^{f_0}\left(x_3\right)}, \tag{23}$$

where $U_1^{2f_0}$ represents the in-plane displacement induced by a crack-related propagating wave at second-order frequency, $U_1^{f_0}$ denotes the in-plane displacement induced by the incident wave. In particular, in the case that the sensor is on the upper surface of the plate, the damage index can be evaluated at the upper surface $x_3 = h$, this yielding

$$NI = \frac{U_1^{2f_0}}{U_1^{f_0}} = \frac{b_1 u_1^{2f_0}\left(h\right)}{b_{Inc} u_1^{f_0}\left(h\right)}. \tag{24}$$

3. PROOF-OF-CONCEPT VALDATION

For proof-of-concept, an aluminum plate, measuring 8 mm in thickness and 1000 mm in length, was considered in numerical simulation. The plate was meshed and analyzed by ABAQUS®/EXPLICIT, to validate the above analytical

modeling. To guarantee the accuracy of numerical simulation, the length of the element was set to ensure that at least 10 elements exist in one wavelength. The properties of the aluminum plate are listed in Table 1.

Table 1 Properties of Aluminum Plate

Density (Kg/m^3)	E (GPa)	υ	c_L (m/s)	c_T (m/s)
2660	71.8	0.33	6324	3185

In order to suppress the influence of dispersive and multimodal properties of GUWs, let the thickness-frequency production of incident wave be 800 kHz.mm. For the discussed crack along the plate thickness, the symmetric propagating mode (S_0) was chosen as the incident wave to make use of its higher sensitivity to this type of crack than an antisymmetric mode, because the in-plane displacement dominates the signal energy. On the left edge of the plate model, five-cycle Hanning-windowed sinusoidal tone bursts were produced by applying the through-thickness displacement field of pure S_0 mode at fundamental frequency. To model the fatigue crack in the plate, the stress-free surfaces of the crack, which are superimposed initially prior to wave traversing, were defined as a seam crack. To facilitate modeling of the CAN, a contact-pair interaction between two crack surfaces was established and the associated properties were defined. A typical moment when the incident GUWs traversing the “breathing” crack is shown in Figure 7

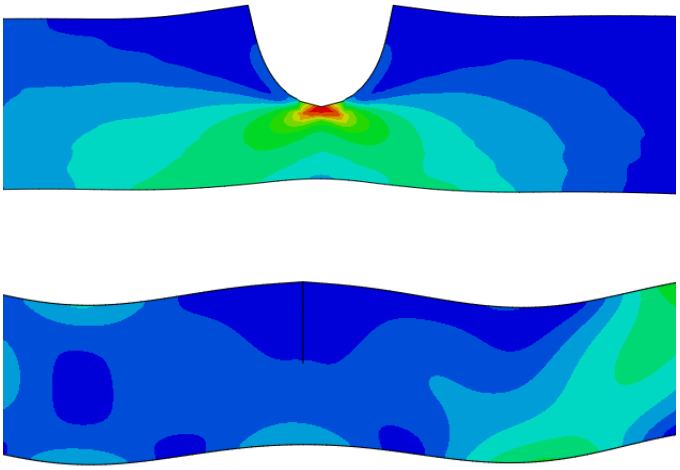

Figure 7. Snapshots of GUWs traversing a breathing crack: (a) tensile stress causing crack open and then stress traversing being interrupted; and (b) compressional stress making crack closed and then stress traversing normally

A typical time-series signal of captured GUWs is shown in the Figure 8(a). Applied with the short-time Fourier Transform (STFT) analysis, the signal spectrum was obtained, as shown in Figure 8(b), from which the time-frequency features were extracted to calculate the nonlinear index using Equation (24). Particular attention was given to the choice of STFT window size so that that time and frequency information of the signal can be retained with sufficient details. From the spectrum, each wave mode can be distinguished and their respective magnitude can be ascertained.

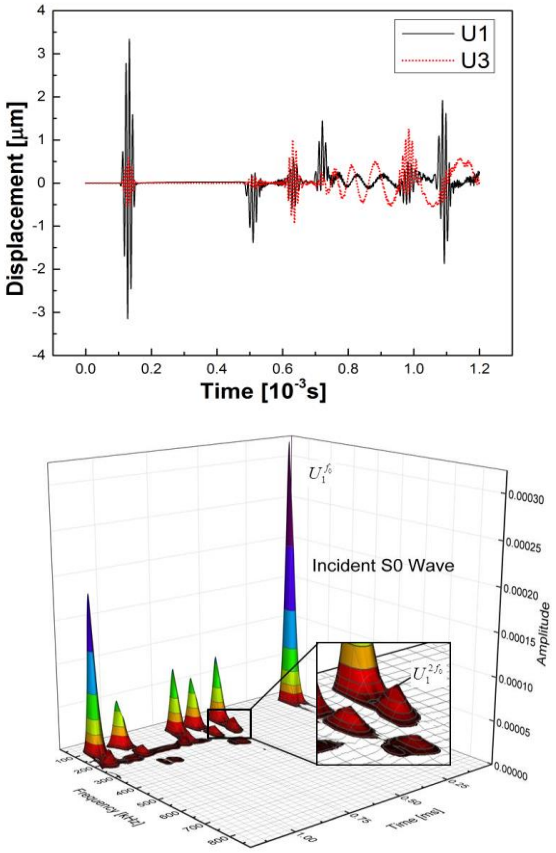

Figure 8. (a) a typical displacement history of a point on the surface of the plate (b) spectrum of the signal shown in (a) using STFT

The accordingly obtained correlation between the nonlinearity index and crack parameters was established, in Figure 9, compared with the results obtained by the proposed analytical method, to observe good coincidence. It can be observed in the Figure 9 that the severer a crack is the larger the defined nonlinear index it will be. From the monotonous correlation shown in Figure 9, conclusion can be drawn that the NI can be used to represent the severity of the crack damage.

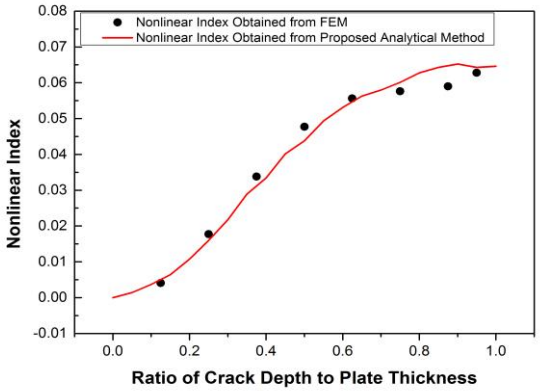

Figure 9. Nonlinearity index against ratio of crack depth to plate thickness

4. DISCUSSIONS AND CONCLUDING REMARKS

In this paper, an analytical model is presented to interpret the modulation mechanism of a "breathing" crack on probing waves and the generation of crack-induced second harmonic generation. In this model, the CAN induced by the "breathing" crack was well interpreted in a 2D scenario by exploiting modal decomposition method and the variational principle. The model defined a second-order harmonic index and established a framework to evaluate the severity of fatigue crack in a quantitative manner by developing correlation between the index and crack parameters. The proposed method was validated by finite element simulation. The comparison shows that based on the results obtained using the proposed method, by measuring the nonlinear features, it is possible to evaluate the severity of the fatigue crack in a quantitative manner. Though effective in simulating and interpreting the influence of a "breathing" crack on wave propagation, the proposed analytical model is foreseen to present some limitations, particularly including the followings:

(1) The proposed method does not take into account the original state of the fatigue crack. For example, in most cases the original gap in between the crack interfaces is non-zero, or the crack is subjected to static compressional stress, under both conditions the crack motion will be influenced intensely;

(2) When a crack grows to a certain extent, the nodes on the crack interfaces do not vibrate in phase, causing different parts of the crack surfaces close at different time, which will influences the generated wave modes heavily and appropriate compensating algorithm is of necessity in order to guarantee the preciseness of results;

(3) It is a challenging job to validate the proposed method by conducting experiments because in a 3D scenario, it is difficult to produce a uniformly deep crack across the width of a plate.

ACKNOWLEDGMENTS

This project is supported by the Hong Kong Research Grants Council via General Research Funds (GRF No. 523313 and No. 15214414). This project is also supported by National Natural Science Foundation of China (Grant No. 51375414).

REFERENCES

[1] W. Ostachowicz and A. Güemes, [New trends in structural health monitoring], Springer Science & Business Media, 542(2013).
[2] D. Balageas, C.-P. Fritzen, and A. Güemes, [Structural health monitoring], Wiley Online Library, 493(2006).
[3] Z. Su and L. Ye, [Identification of damage using Lamb waves: from fundamentals to applications], Springer Science & Business Media, 48(2009).
[4] A. Raghavan and C. E. Cesnik, "Review of guided-wave structural health monitoring," Shock and Vibration Digest 39, 91-116 (2007).
[5] Y. Lu, L. Ye, Z. Su, and N. Huang, "Quantitative evaluation of crack orientation in aluminium plates based on Lamb waves," Smart Materials and Structures 16, 1907 (2007).
[6] M. Meo and G. Zumpano, "Nonlinear elastic wave spectroscopy identification of impact damage on a sandwich plate," Composite structures 71, 469-474 (2005).
[7] J. H. Cantrell, "Quantitative assessment of fatigue damage accumulation in wavy slip metals from acoustic harmonic generation," Philosophical Magazine 86, 1539-1554 (2006).
[8] G. Zumpano and M. Meo, "A new nonlinear elastic time reversal acoustic method for the identification and localisation of stress corrosion cracking in welded plate-like structures–A simulation study," International journal of solids and structures 44, 3666-3684 (2007).

[9] G. Zumpano and M. Meo, “Damage localization using transient non-linear elastic wave spectroscopy on composite structures,” International Journal of Non-Linear Mechanics 43, 217-230 (2008).
[10] C. Zhou, M. Hong, Z. Su, Q. Wang, and L. Cheng, “Evaluation of fatigue cracks using nonlinearities of acousto-ultrasonic waves acquired by an active sensor network,” Smart Materials and Structures 22, 015018 (2012).
[11] M. F. Müller, J.-Y. Kim, J. Qu, and L. J. Jacobs, “Characteristics of second harmonic generation of Lamb waves in nonlinear elastic plates,” The Journal of the Acoustical Society of America 127, 2141-2152 (2010).
[12] C. Bermes, J.-Y. Kim, J. Qu, and L. J. Jacobs, “Nonlinear Lamb waves for the detection of material nonlinearity,” Mechanical Systems and Signal Processing 22, 638-646 (2008).
[13] J. Pei and M. Deng, “Assessment of fatigue damage in solid plates using ultrasonic lamb wave spectra,” Ultrasonics Symposium, 2008. IUS 2008. IEEE,1869-1872 (2008).
[14] C. Pruell, J.-Y. Kim, J. Qu, and L. J. Jacobs, “Evaluation of fatigue damage using nonlinear guided waves,” Smart Materials and Structures 18, 035003 (2009).
[15] J.-Y. Kim, L. J. Jacobs, J. Qu, and J. W. Littles, “Experimental characterization of fatigue damage in a nickel-base superalloy using nonlinear ultrasonic waves,” The Journal of the Acoustical Society of America 120, 1266-1273 (2006).
[16] I. Y. Solodov, N. Krohn, and G. Busse, “CAN: an example of nonclassical acoustic nonlinearity in solids,” Ultrasonics 40, 621-625 (2002).
[17] K. Dziedziech, L. Pieczonka, P. Kijanka, and W. J. Staszewski, “Enhanced nonlinear crack‐wave interactions for structural damage detection based on guided ultrasonic waves,” Structural Control and Health Monitoring, (2016).
[18] Z. Parsons and W. Staszewski, “Nonlinear acoustics with low-profile piezoceramic excitation for crack detection in metallic structures,” Smart Materials and Structures 15, 1110 (2006).
[19] A. Klepka, W. Staszewski, R. Jenal, M. Szwedo, J. Iwaniec, and T. Uhl, “Nonlinear acoustics for fatigue crack detection–experimental investigations of vibro-acoustic wave modulations,” Structural Health Monitoring 11, 197-211 (2012).
[20] S. Pavlopoulou, W. Staszewski, and C. Soutis, “Evaluation of instantaneous characteristics of guided ultrasonic waves for structural quality and health monitoring,” Structural Control and Health Monitoring 20, 937-955 (2013).
[21] M. Castaings, E. Le Clezio, and B. Hosten, “Modal decomposition method for modeling the interaction of Lamb waves with cracks,” The Journal of the Acoustical Society of America 112, 2567-2582 (2002).
[22] X.-M. Wang and C. Ying, “Scattering of Lamb waves by a circular cylinder,” The Journal of the Acoustical Society of America 110, 1752-1763 (2001).
[23] P. Kirrmann, “On the completeness of Lamb modes,” Journal of elasticity 37, 39-69 (1994).
[24] P. J. Torvik, “Reflection of Wave Trains in Semi‐Infinite Plates,” The Journal of the Acoustical Society of America 41, 346-353 (1967).
[25] R. Mindlin, “Investigations in the mathematical theory of vibrations of anisotropic bodies,” U „S. Army Signal Corps Eng. Labs., Fort Monmouth, NJ, 84ff (1956).